The Astrophysical Journal, 706:1438–1450, 2009 December 1 doi:10.1088/0004-637X/706/2/1438

MAGNETIC RECONNECTION DURING THE TWO-PHASE EVOLUTION OF A SOLAR ERUPTIVE FLARE

Bhuwan Joshi[1,2], Astrid Veronig[3], K.-S. Cho[1], S.-C. Bong[1], B. V. Somov[4], Y.-J. Moon[5], Jeongwoo Lee[6], P. K. Manoharan[7], and Y.-H. Kim[1]

[1] Korea Astronomy and Space Science Institute, Daejeon 305-348, Korea; bhuwan@prl.res.in
[2] Udaipur Solar Observatory, Physical Research Laboratory, Udaipur 313 001, India
[3] IGAM/Institute of Physics, University of Graz, Universitätsplatz 5, A-8010 Graz, Austria
[4] Astronomical Institute, Moscow State University, Universitetskij Prospekt 13, Moscow 119992, Russia
[5] School of Space Research, Kyung Hee University, Yongin 446-701, Korea
[6] Physics Department, New Jersey Institute of Technology, 161 Warren Street, Newark, NJ 07102, USA
[7] Radio Astronomy Centre, Tata Institute of Fundamental Research, Udhagamandalam (Ooty) 643 001, India
Received 2008 July 22; accepted 2009 October 14; published 2009 November 12

ABSTRACT

We present a detailed multi-wavelength analysis and interpretation of the evolution of an M7.6 flare that occurred near the southeast limb on 2003 October 24. Pre-flare images at TRACE 195 Å show that the bright and complex system of coronal loops already existed at the flaring site. The X-ray observations of the flare taken from the *Reuven Ramaty High Energy Solar Spectroscopic Imager* (*RHESSI*) spacecraft reveal two phases of the flare evolution. The first phase is characterized by the altitude decrease of the X-ray looptop (LT) source for ∼11 minutes. Such a long duration of the descending LT source motion is reported for the first time. The EUV loops, located below the X-ray LT source, also undergo contraction with similar speed (∼15 km s^{-1}) in this interval. During the second phase the two distinct hard X-ray footpoint (FP) sources are observed which correlate well with UV and Hα flare ribbons. The X-ray LT source now exhibits upward motion as anticipated from the standard flare model. The *RHESSI* spectra during the first phase are soft and indicative of hot thermal emission from flaring loops with temperatures $T > 25$ MK at the early stage. On the other hand, the spectra at high energies ($\varepsilon \gtrsim 25$ keV) follow hard power laws during the second phase ($\gamma = 2.6$–2.8). We show that the observed motion of the LT and FP sources can be understood as a consequence of three-dimensional magnetic reconnection at a separator in the corona. During the first phase of the flare, the reconnection releases an excess of magnetic energy related to the magnetic tensions generated before a flare by the shear flows in the photosphere. The relaxation of the associated magnetic shear in the corona by the reconnection process explains the descending motion of the LT source. During the second phase, the ordinary reconnection process dominates describing the energy release in terms of the standard model of large eruptive flares with increasing FP separation and upward motion of the LT source.

Key words: Sun: corona – Sun: flares – Sun: X-rays, gamma rays

Online-only material: color figures

1. INTRODUCTION

The active Sun displays a stunning variety of transient energetic phenomena ranging from the smallest microjets and microflares to the largest flares and coronal mass ejections (CMEs). It is generally accepted that the energy released during flares and CMEs is stored in the corona prior to the event in the form of stressed or non-potential magnetic fields. We believe that this stored free energy in the coronal magnetic fields is released explosively through the process of magnetic reconnection. Multi-wavelength measurements of flares and CMEs made over the years have provided many valuable pieces of information about the response of coronal energy release in the different atmospheric layers of the Sun. During an eruptive flare, the whole magnetic configuration of coronal loops crossing an inversion line is disrupted and is followed by a newly rebuilt loop system from pre-flare to post-flare stages. The expansion of flare ribbons and growth of flare loop system are the clearest observational findings which support the flare models involving magnetic reconnection (for a review see Priest & Forbes 2002; Lin et al. 2003).

Yohkoh spacecraft significantly improved our overall understanding about the flare physics (Hudson et al. 2004). Observations made by Yohkoh confirmed the presence of hard X-ray (HXR) sources at the footpoints (FPs) of the loop system (Sakao 1994) and detected a new HXR source above the apex of the hot flaring loop observed in soft X-rays (Masuda et al. 1994; Somov et al. 2005a). The above-the-looptop source is believed to be intimately connected to the primary energy release site and location of the electron acceleration in the corona, again supporting the reconnection models. *Reuven Ramaty High Energy Solar Spectroscopic Imager* (*RHESSI*) spacecraft with superior observing capabilities in X-ray energy levels, further refined our knowledge about the X-ray looptop (LT) coronal sources (see review by Krucker et al. 2008). It detected a downward motion of the LT source during the initial phase of impulsive rise of HXR flux (Sui & Holman 2003; Sui et al. 2004; Liu et al. 2004; Ji et al. 2006; Veronig et al. 2006; Joshi et al. 2007). We still do not have a plausible explanation of this phenomenon. *RHESSI* observations have also revealed the existence of double coronal sources (Sui & Holman 2003; Sui et al. 2004, 2005; Veronig et al. 2006; Li & Gan 2007; Liu et al. 2008). The double coronal source has been interpreted as an indirect evidence for the formation and expansion of a large-scale current sheet in the corona (Sui & Holman 2003; Sui et al. 2004, 2005).

In this paper, we present a comprehensive multi-wavelength analysis of an M7.6 flare on 2003 October 24. A detailed X-ray imaging and spectroscopic analysis of *RHESSI* observations exhibit two phases of flare evolution in view of the X-ray energy release process. A significant and unusually long downward

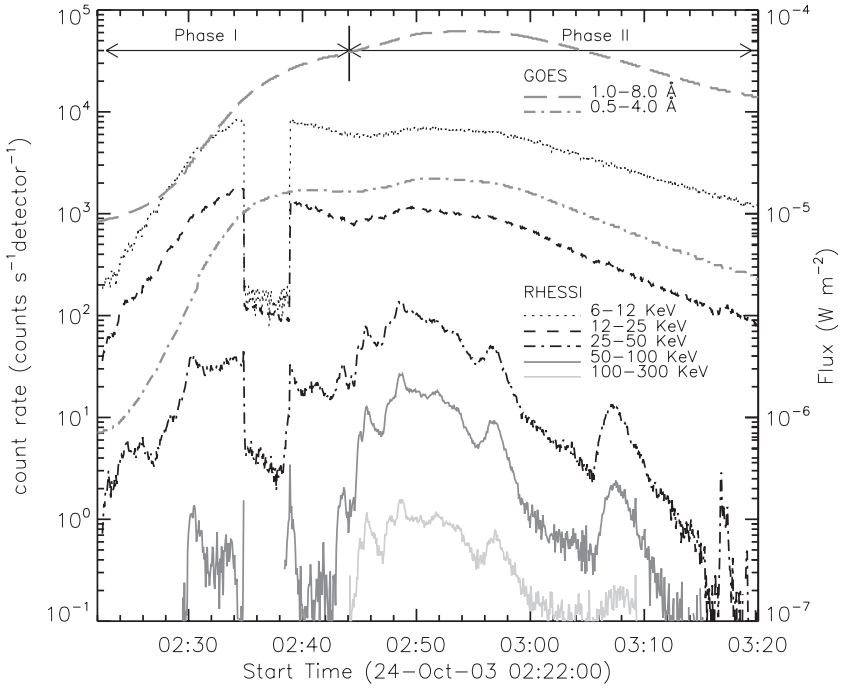

Figure 1. *RHESSI* and *GOES* light curves of the flare. *RHESSI* counts rates are averaged over every 4 s. In order to present different *RHESSI* light curves with clarity, the *RHESSI* count rates are scaled by factors of 1, 1/4, 1/5, 1/10, and 1/50 for the energy bands 6–12, 12–25, 25–50, 50–100, and 100–300 keV, respectively.

motion of the LT source characterizes the first phase. During the whole second phase we observe FP sources and upward expansion of the LT source, as it is commonly observed in solar flares. The event was associated with a fast CME. We compare flare observations at different X-ray wavelengths, and also with other chromospheric and coronal images with the aim to study the consequences of the magnetic reconnection process at various atmospheric layers. In Section 2, we describe the observational characteristics of the event. We interpret our observational findings in the final section of the paper.

2. OBSERVATIONS AND RESULTS

2.1. X-ray Time Profiles: Two-phase Evolution

The soft X-ray fluxes recorded by the *GOES* satellite in the 0.5–4 and 1–8 Å wavelength bands reveal this flare to be a typical long duration event lasting from 02:15 to about 05:00 UT. The *GOES* flux in the 0.5–4 Å channel attained the first peak at 02:40 UT (Figure 1). The flux then shows a decreasing trend and then further increases after 02:44 UT. The overall maximum is achieved in both *GOES* channels at 02:53 UT.

The *RHESSI* (Lin et al. 2002) made a complete coverage of this long duration event. However, X-ray counts were contaminated by counts produced by radiation belt particles hitting the *RHESSI* detectors from all the directions. Particle events mainly affect the X-ray count rate at high energies ($\geqslant$ 40 keV). In order to obtain the X-ray fluxes free from particle contamination we adopted the method described in Liu et al. (2009a). For the background estimation we selected a non-flare interval 04:30:30–04:33:00 on 2003 October 24, when the spacecraft was at approximately same geomagnetic location during its next orbit. The corrected X-ray count rates averaged over front detectors 1, 3–6, 8, and 9 in the 6–12, 12–25, 25–50, 50–100, and 100–300 keV energy bands are shown in Figure 1.

The inspection of *GOES* and *RHESSI* ($\leqslant$25 keV) time profiles shows two phases of the flare evolution: a first phase between 02:24 and 02:44 UT, followed by a second phase. However, the X-ray light curves at high energy bands ($\geqslant$ 25 keV) reveal that the emission during the second phase is much stronger than the first phase. Here it is relevant to mention that the X-ray and EUV images further confirm two-phase distinction in terms of the morphological evolution of the flare (Section 2.2).

It is noteworthy that the LASCO instrument onboard *SOHO* (Brueckner et al. 1995) detected a fast CME associated with this flare event. The height–time plot available at *SOHO*–LASCO–CME catalogue[8] shows the mean propagation speed of CME in LASCO field of view to be about 1055 km s^{-1}. The CME first appeared in the LASCO C2 coronagraph at 02:54 UT at a radial distance of $\sim$2.7 $R_{\odot}$. The extrapolation of CME height backward in time suggests its association with the first phase of the flare evolution.

2.2. X-ray, (E)UV, and Hα Imaging

The *RHESSI* images have been reconstructed with the CLEAN algorithm with the natural weighing scheme using front detector segments 3–8 in different energy bands, namely, 6–12, 10–15, 25–50, 50–100, and 100-300 keV (Hurford et al. 2002). We compare *RHESSI* measurements with TRACE images in 195 and 1600 Å wavelengths. The *TRACE* 1600 Å channel is sensitive to plasma in the temperature range between (4–10) $\times$ 10^3 K. Emissions at this wavelength originate mainly from the chromosphere and provide valuable informations about the chromospheric response to the coronal energy release. The TRACE 195 Å filter is mainly sensitive to plasmas at a temperature around 1.5 MK (Fe XII) but during flares it may also contain significant contributions of plasmas at temperatures around 15–20 MK (due to an Fe XXIV line; Handy et al. 1999).

It is well known that TRACE images do not have accurate absolute pointing. However, the pointing information of *RHESSI*

[8] http://cdaw.gsfc.nasa.gov/CME_list/

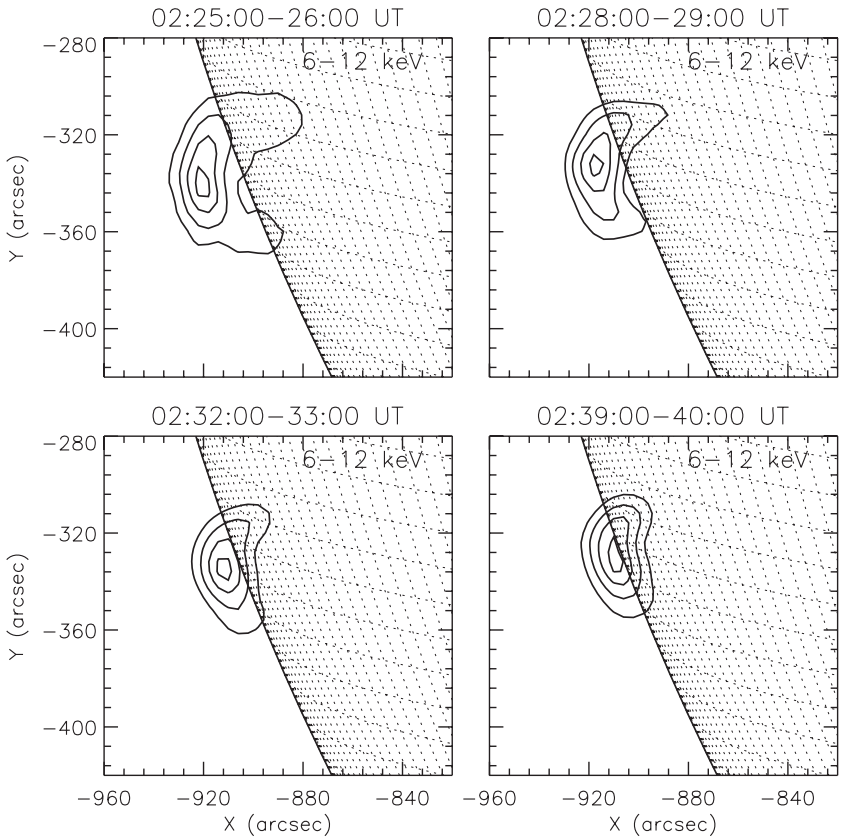

Figure 2. Sequence of *RHESSI* 6–12 keV images reconstructed with the CLEAN algorithm using grids 3–8 and natural weighing scheme during the first phase of the flare showing the altitude decrease of the flaring loop system. The integration time for each image was 1 minute. The contour levels are 40%, 60%, 80%, and 95% of the peak flux in each image. The solar limb and heliographic grids are also drawn in each panel.

and *SOHO* is believed to be accurate. Therefore we corrected TRACE pointing by a cross-correlation alignment between a TRACE and a *SOHO*/EIT image observed at 02:23:30 and 02:24:38 UT, respectively, in the 195 Å channel. For the cross correlation, we used the Solar SoftWare (SSW) routine, trace_mdi_align, developed by Metcalf (see also Metcalf et al. 2003).

First, we discuss the flare characteristics during the first phase of evolution (i.e., between 02:24 and 02:44 UT) prominent in *GOES* profile and *RHESSI* measurements at low energies ($\lesssim$ 25 keV). *RHESSI* images reconstructed in various energy bands below 50 keV show a bright LT source which develops right at the flare onset. The LT source then shows shift to lower altitudes. In Figure 2, four representative 6–12 keV images during this period are shown. At the flare onset, an LT source and associated coronal loop are seen. The LT source appeared above the limb while the loop system extends to the disk with northern leg apparently longer than the southern one (top left panel of Figure 2). In the later stages, the loop system shrinks and the LT structure continues to become more compact and brighter.

A bright and complex system of parallel loops already pre-existed and was observable in TRACE 195 Å images at the activity site before the flare onset (first panel of Figure 3). *RHESSI* LT source, which appeared as early as ∼02:24 UT, is located above the northern side of the TRACE loop system (Figure 4). Intense brightening occurred at the top of TRACE loops from 02:29 UT onward and the loops start shrinking (Figure 3).

In Figure 5, we present the altitude evolution of the LT source derived from *RHESSI* images in three energy bands, namely 6–12, 12–25, and 25–50 keV, and TRACE 195 Å images. Here, the LT altitude is defined as the distance, along the main axis of motion, between the centroid of LT and the center of the line between the two FPs seen in *RHESSI* 50–100 keV energy band image at 02:51:00 UT. The axis of motion is determined by fitting a straight line to the centroids of the LT source and is inclined at an angle of 25° northward from the radial *x*-axis. For *RHESSI* images, we have taken the centroid of emission of all pixels above 85% of the peak flux. The TRACE LT is defined by selecting a region near the top of loop with emission above 90% of the peak flux of each image. We find that the *RHESSI* LT sources observed at 6–12, 12–25, and 25–50 keV energy bands are almost co-spatial during the whole first phase and descend with similar velocities between 02:25 and 02:35 UT (∼15 km s^{-1}). The TRACE LT source, located below the X-ray LT source, also shows similar velocity of downward motion in this interval. *RHESSI* and TRACE images provide a consistent picture of the loop shrinkage during the first phase.

RHESSI images during the second phase of the flare (i.e., between 02:44 and 03:10 UT) show the expansion of flare loop at low energies ($\lesssim$25 keV), and the origin and evolution of the HXR sources on the solar disk at high energies ($\gtrsim$25 keV). Figure 6 presents a few representative images in 10–15 and 50–100 keV energy bands. The X-ray light curve above 25 keV shows peaks at the time of these images (Figure 1). A HXR source appeared around the peak at ∼02:45 UT. Another source developed southward to the first one at 02:48 UT, the time of flare maximum observed in *RHESSI* light curves above 25 keV. These two sources lie over the two bright flare ribbons observed at 1600 Å TRACE images (Figure 8). Therefore, we interpret

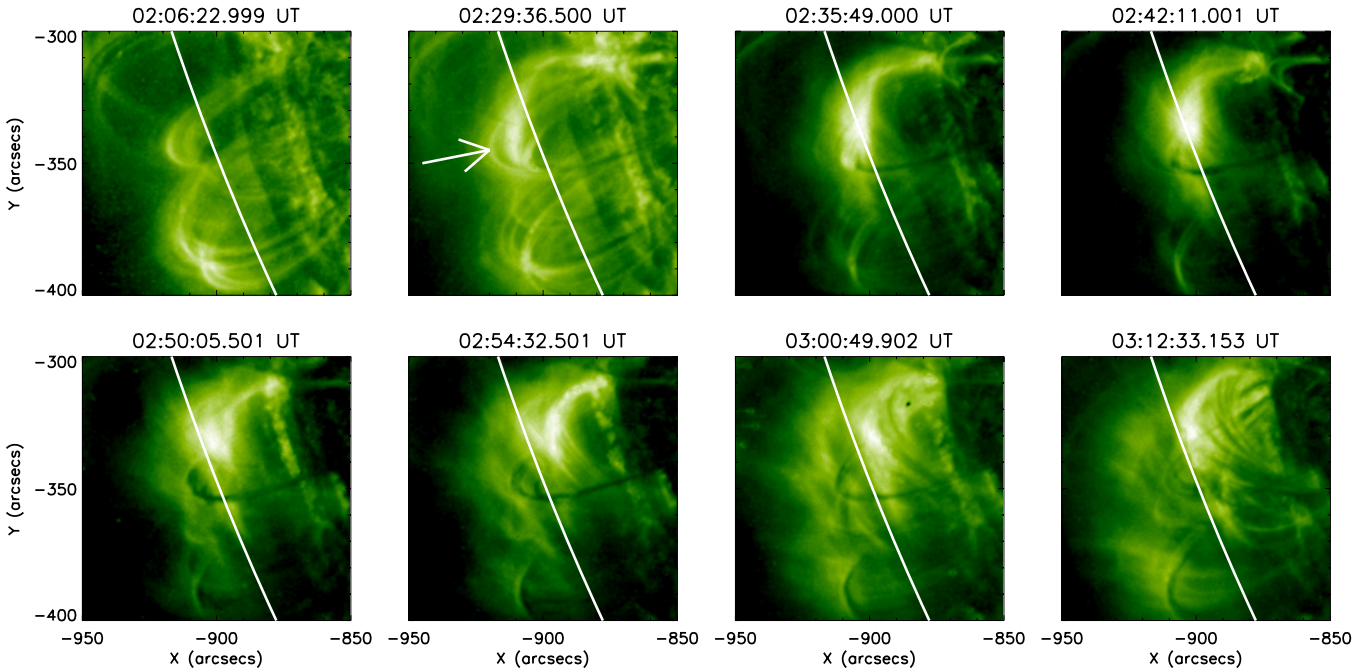

Figure 3. Time sequence of TRACE 195 Å images showing a closer view of coronal loops associated with the flaring region. The bright region at the top of the loop system is indicated by an arrow in the image at 02:29:36 UT. Note the pre-existing loop system and altitude decrease of the flaring loops at the first flare phase, followed by ($\gtrsim$ 2:54 UT) post-flare loops appearing dark and structured.

(A color version of this figure is available in the online journal.)

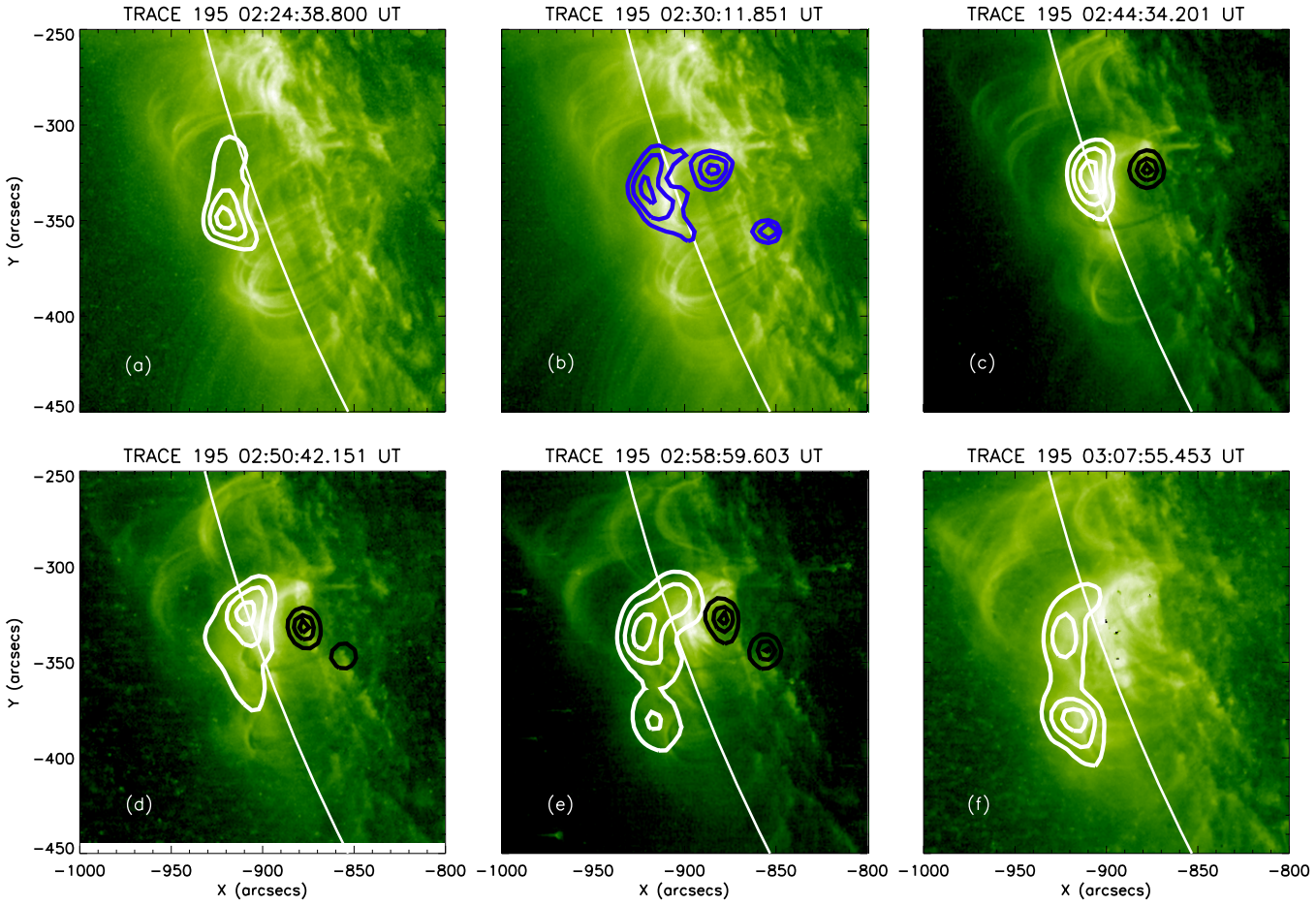

Figure 4. Sequence of TRACE 195 Å images overlaid by co-temporal *RHESSI* X-ray images. *RHESSI* image parameters are the same as in Figure 2. Panels (a)–(f) (except (b)): 6–12 keV (white contours) and 50–100 keV (black contours) images are plotted with contour levels 50%, 70%, and 90% of the peak flux in each image. Panel (b): 25–50 keV image (blue contours) is plotted with contour levels 65%, 80%, and 95% of the peak flux.

(A color version of this figure is available in the online journal.)

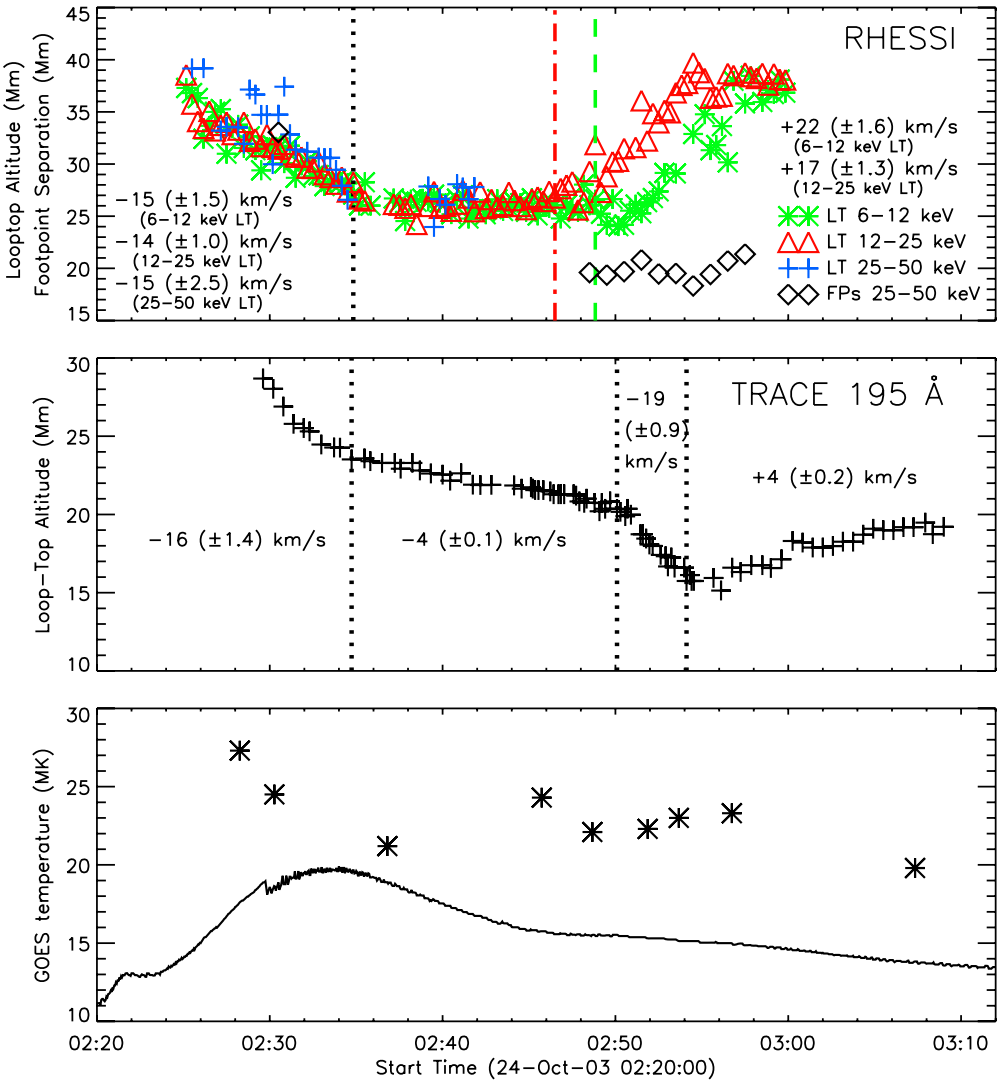

Figure 5. Evolution of the altitude of the *RHESSI* LT source observed in the 6–12, 12–25, and 25–50 keV energy bands. Note that the *RHESSI* LT source at 12–25 and 6–12 keV show upward motion after ∼02:46 and ∼02:49 UT respectively (start time is indicated by dash-dotted and dashed lines, respectively). The FP separation derived from *RHESSI* 25–50 keV images is also plotted. Middle panel: evolution of the altitude of the TRACE 195 Å LT source. The mean velocities derived by linear fits to the altitude data in certain time interval (indicated by vertical lines) are annotated in the Figure. Bottom panel: time profile of temperature derived from *GOES*-12 measurements. The data points denoted by asterisk symbols show the plasma temperature estimated from *RHESSI* measurements.

(A color version of this figure is available in the online journal.)

these two sources as the northern and southern FPs of a loop system, the LT of which is clearly visible in *RHESSI* images at low energies (Figures 6 and 8). We note that most of the time the northern FP remains brighter than the southern one. However, the intensity of the southern FP increases slowly with time and near the end of the second phase both the FPs are of similar brightness.

We note that the evolution of the LT source after 02:35 UT is rather complicated. Examination of both 6–12 and 12–25 keV images shows that the height of LT source does not change for the next few minutes before showing the commonly observed upward expansion (Figure 5). The X-ray LT source at 12-25 keV starts moving upward ∼3 minutes earlier than the 6-12 keV source. We also notice that during the upward expansion, the LT source at 12–25 keV is located at higher altitudes than the LT source in 6–12 keV (i.e., the emission at higher X-ray energies originates from higher altitude). For upward motion, we obtained mean velocities of 22 and 17 km s^{-1} for 6–12 (between 02:49 and 03:00 UT) and 12–25 keV (between 02:46 and 03:00) sources, respectively. Another interesting feature during the upward motion of the X-ray LT source is the increase in the brightness at the top of a nearby loop system (seen in TRACE 195 Å images; see image at 02:58:59 UT in Figure 4) situated at the southern side of the main LT source. In the later stages, the brightness of southern LT source increases and start dominating over the northern main LT source. The TRACE 195 Å LT source with bright, diffuse emission exhibits little downward motion between 02:35 and 02:50 UT (Figures 3 and 5) with a mean velocity of 4 km s^{-1}. In the later stages (> 02:54 UT), the bright emission seen in TRACE 195 Å images is more structured and spread along the loop, below which a dark (and cool) system of post-flare loops is visible (Figure 3). The loop system shows an upward expansion with a mean velocity of 4 km s^{-1}.

Here it is important to discuss a few observational features seen in the X-ray light curve and images for 25–50 keV energy bands in detail (Figures 1 and 7). There is a sharp rise in the X-ray flux from 02:27 UT which attains a maximum level at 02:30 UT.

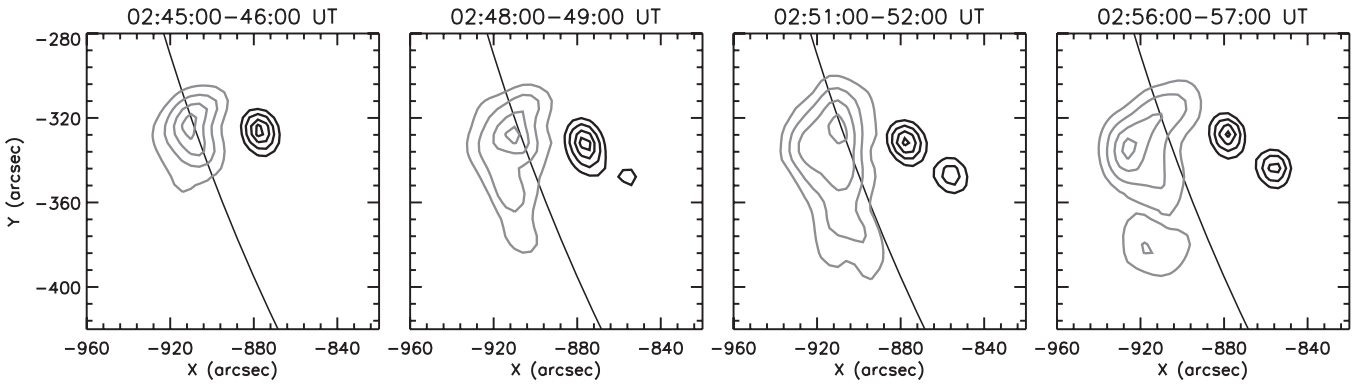

Figure 6. Sequence of *RHESSI* 10–15 keV (gray contours) and 50–100 keV (black contours) images showing the evolution of LT and FP sources, respectively. The image reconstruction parameters are the same as in Figure 2. The contour levels are 40%, 60%, 80%, and 95% of the peak flux in each image.

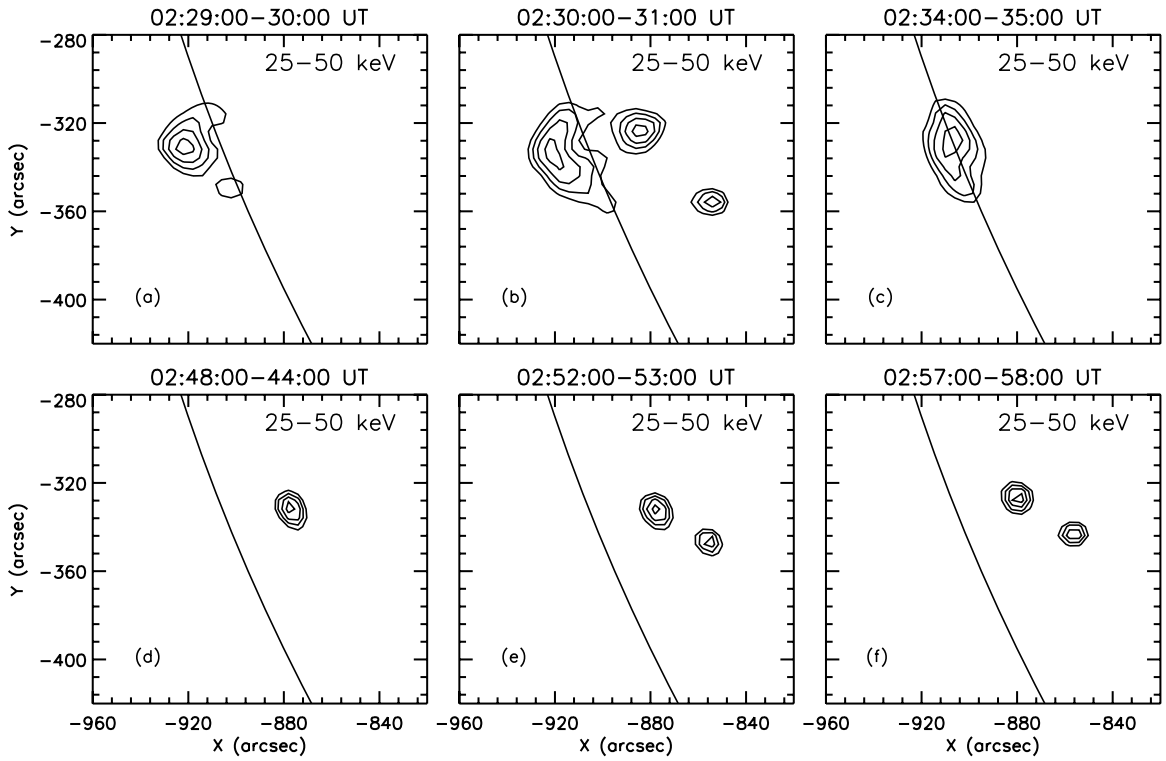

Figure 7. Sequence of *RHESSI* 25–50 keV images. The contour levels are 65%, 75%, 85%, and 95% of the peak flux in each image. Note the two bright FP sources at 02:30:00-02:31:00 UT appeared for a short period during the prolonged preheating phase when the LT source shows a descending motion. On the other hand, two conjugate FPs can be seen during the second phase from 02:52 UT onward (see panel e). In this phase, the LT source moves upward (see Figure 6). It is noteworthy that the separation between the two FPs during the first phase (panel b) is larger than that during the second phase (panel e).

The flux maintains nearly a constant level for the next few minutes and shows a gradual decline till ∼02:43 UT. The images during this interval show a descending LT source, similar to the LT source observed at energies below 25 keV. However, for a brief period of time, 02:30–02:31 UT, two bright and distinct FP sources are observed in addition to the LT source (Figure 7(b)). The 25–50 keV images during the second phase show only FP sources and its evolution is similar to the FP sources seen at higher energies ($\geqslant$ 50 keV). In Figure 5 (top panel) we also show the separation of the two X-ray FPs reconstructed at 25–50 keV energies. The two distinct FPs, observed between 02:48 and 02:57 UT, separate from each other with an average speed of ∼2 km s^{-1}. We also find that the speed of separation increases at later stages (∼7 km s^{-1} between 02:52 and 02:57 UT). We further note that the separation between the two FPs in the first phase (which is observed only in one image at 02:30–02:31) is larger than the FP separation observed in the second phase (see Figures 7(b) and 7(e)).

In the bottom panel of Figure 5, we have shown the temporal evolution of plasma temperature derived from *GOES* 12 observations. We find that the plasma temperature is higher during the first phase and attains the maximum value at ∼02:34 UT. Further we find that the decrease of the LT source altitude is anti-correlated with plasma temperature evolution during the first phase (between 02:24 and 02:35 UT). After 02:34 UT plasma temperature decreases rapidly till ∼02:44 UT. In the beginning of the second phase the temperature remains nearly constants for several minutes (between ∼02:47 and ∼02:53 UT) while it decreases very slowly in the later stages.

The TRACE images at 1600 Å and Hα filtergrams taken from ARIES Solar Tower Telescope, India (Pant 2006) during the decline phase (after 02:55 UT) reveal clear post-flare loop

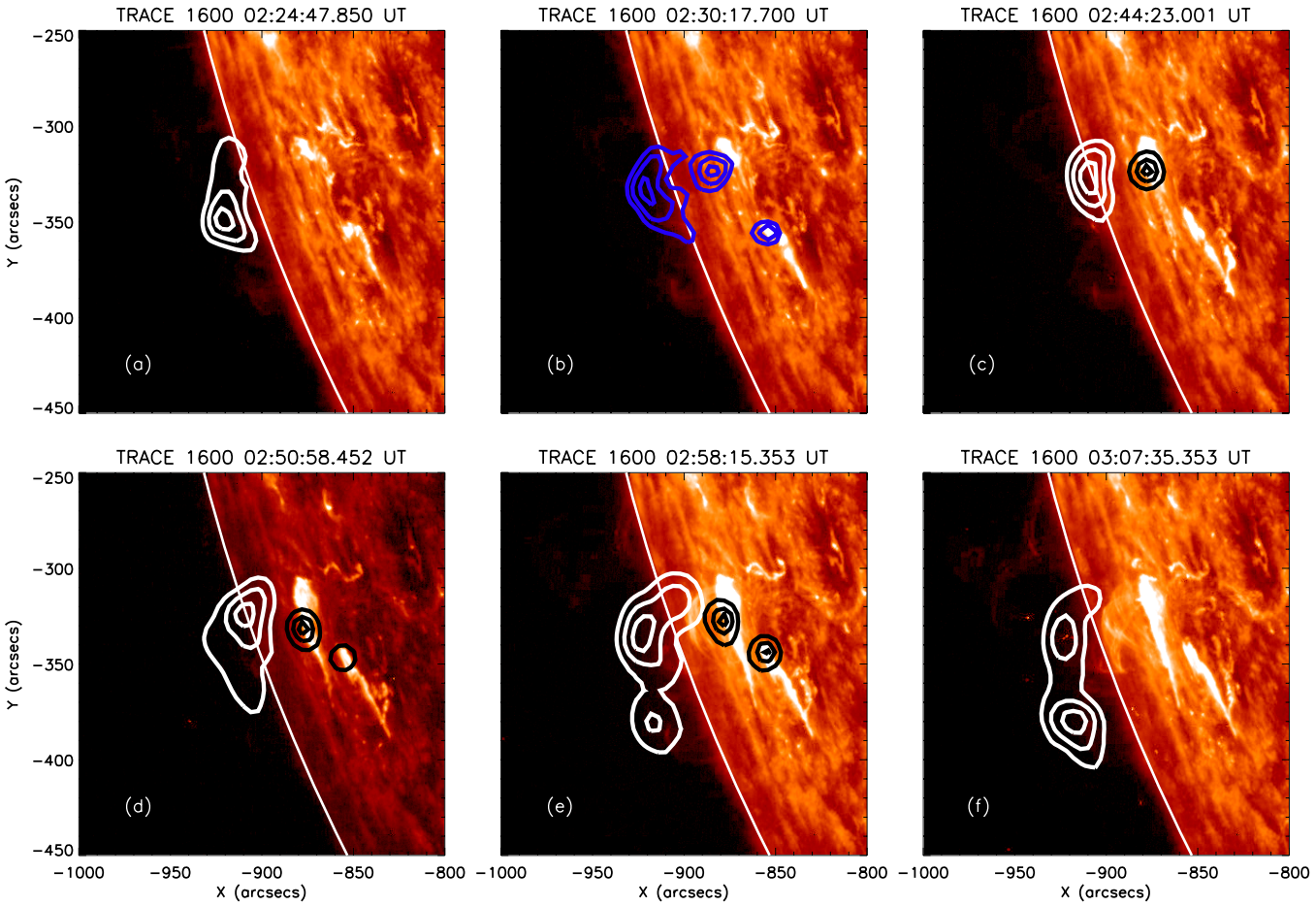

Figure 8. Sequence of TRACE 1600 Å images overlaid by co-temporal *RHESSI* X-ray images. *RHESSI* image parameters are the same as in Figure 2. Panels (a)–(f) (except (b)): 6–12 keV (white contours) and 50–100 keV (black contours) images are plotted with contour levels 50%, 70%, and 90% of the peak flux in each image. Panel (b): 25–50 keV image (blue contours) is plotted with contour levels 65%, 80%, and 95% of the peak flux.

(A color version of this figure is available in the online journal.)

configuration that connects the flare ribbons (Figures 8 and 9). We further note that the Hα loops are seen in emission against the solar disk which is not a commonly observed phenomenon.

2.3. RHESSI *X-ray Spectroscopy*

Figure 10 shows spatially integrated, background-subtracted *RHESSI* spectra derived during nine time intervals of the flare together with the applied spectral fits. Each spectrum was accumulated over 80 s and derived with 1 keV energy bins from 10 to 200 keV using all *RHESSI* front detector segments except 2 and 7 (which have lower energy resolution and high threshold energies, respectively) and deconvolved with the full detector response matrix, i.e., including off-diagonal elements (see Smith et al. 2002). Due to the high count rates at low energies, the effect of pile-up may be significant during this event, i.e., two (or more) low-energy photons arrive almost simultaneously at one detector and are recorded as a single photon with energy equal to the sum of the individual photon energies (Smith et al. 2002). Detector live time is the simplest indicator for a quantitative understanding of the pile-up effect. We obtained live time averaged over the seven detectors being used. The spectra shown in the top row of Figure 10 were derived during the first phase of the flare. The average live time for these three time intervals was 92%, 86%, and 97% respectively. We find that for the third interval the pile-up effect is smallest (detector live times are 97%) because it is in the A3 attenuator state. During the second phase we obtained spectra for six time intervals (middle and bottom rows of Figure 10) with average live times of 83%, 81%, 81%, 81%, 83%, and 91% respectively. We note that the spectra derived during the interval 02:48:00–02:49:20 UT cover the impulsive phase for which the average live time was 81%. In general, the live time values are relatively lower and indicate moderate pile-up severity. For example, the average live time for the M1.7 flare on 2003 November 13 during the impulsive phase was ranging from 96% to 89% (Liu et al. 2006). We applied the pile-up correction implemented in the *RHESSI* software. However, we note that during the early phase (Figure 10, top row) where the spectra are very steep, this correction may not be fully satisfactory.

Spectral fits were obtained using a forward-fitting technique for which the functional form of the incident photon flux spectra is assumed for a parametric model of the source. Specifically, we used the bremsstrahlung spectrum of an isothermal plasma and a power-law function with a turn-over at low X-ray energies. The spectra during the first phase of the flare (top row of Figure 10) suggest hot thermal emission with temperatures $T > 25$ MK already at the very start. At X-ray energies $\varepsilon \gtrsim 20$ keV, the spectrum shows a steep power law, with photon spectral index $\gamma \gtrsim 7$. At this first phase of the flare, *RHESSI* images show emission mostly from the flaring loops, concentrated toward the LTs. Only during one interval at 02:30–02:31 UT we briefly see HXR emission from FPs (in 25–50 keV *RHESSI* images,

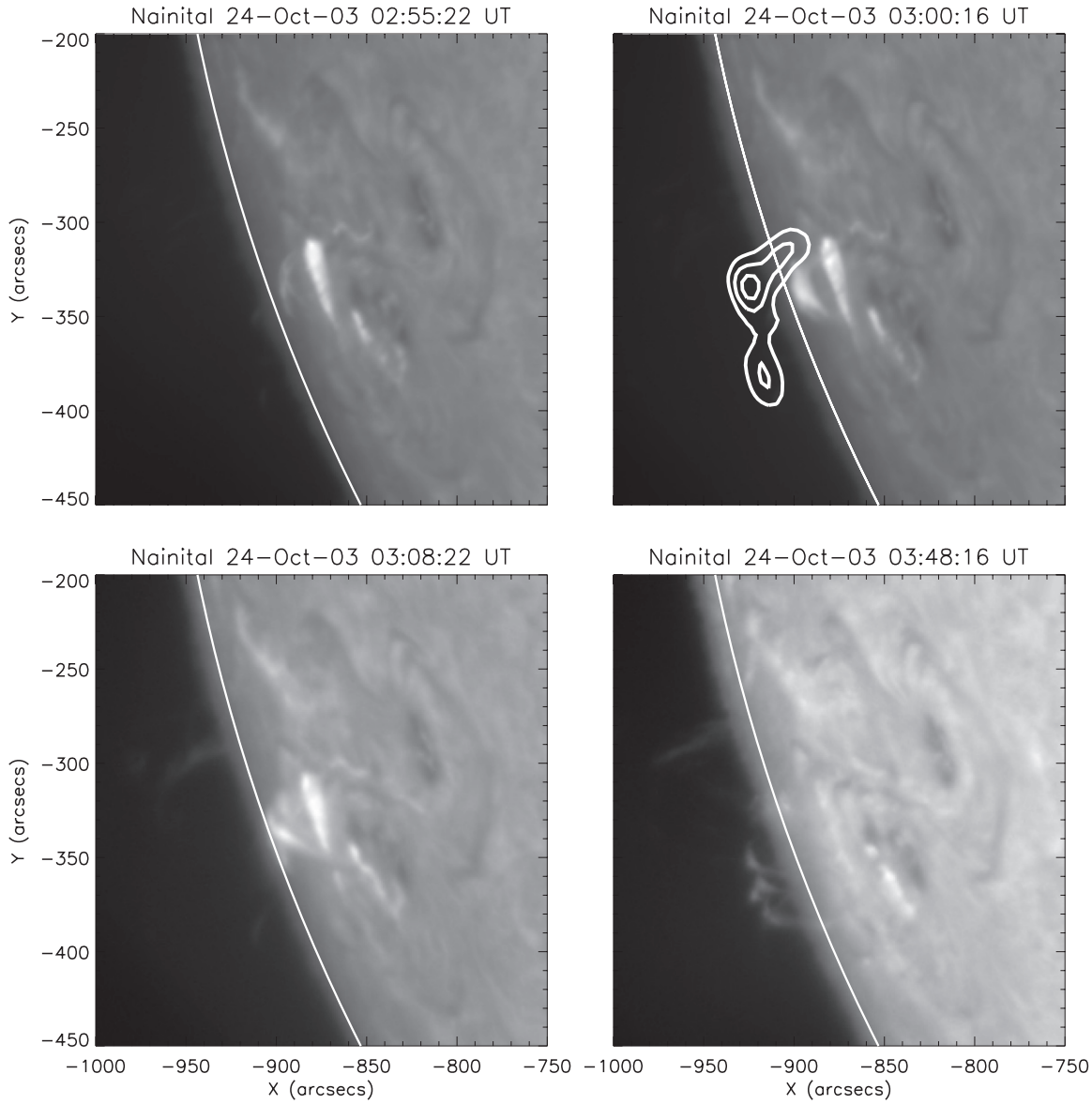

Figure 9. Some representative Hα images during the decline phase of the event. The white contours (only in top right panel) are *RHESSI* 6–12 keV image. The contour levels are 50%, 70%, and 90% of the peak flux. Note that the Hα post-flare loops appearing bright against the disk, implying high plasma densities in the loops.

Figure 7). At this time also the spectral index is harder with $\gamma = 5.7$ (see the middle panel of top row in Figure 10).

During the second phase of the flare, the spectra show quite different characteristics (see middle and bottom rows of Figure 10). Emission up to >200 keV from *RHESSI* FPs is detectable above the background, and the spectrum at high energies follows hard power laws (with photon spectral index γ in the range 2.5–2.8 during the individual peaks). We note that the thermal emission does not increase any further in this second flare phase but temperature as well as emission measure has reached their peaks already during the first phase.

3. DISCUSSION AND INTERPRETATION

3.1. The First Phase

Pre-flare images of the active region taken by TRACE at 195 Å show that a bright and complex system of coronal loops has already existed in the flaring region. The X-ray and EUV observations during the first phase of flare evolution reveal many important observational findings. The X-ray LT source appeared right at the flare onset and starts moving to lower altitudes. The LT source is characterized by an unusually long duration of altitude decrease (from 02:24 to 02:35 UT). About 5 minutes after the appearance of X-ray LT source, an intense and diffuse brightening is observed at the top of TRACE 195 Å loops, located below the *RHESSI* LT source. Warren & Reeves (2001) and Gallagher et al. (2002) reported very similar bright and diffuse emission from TRACE 195 Å loops associated with X-class flares, which was interpreted as being due to the Fe XXIV contribution of plasma at a temperature of 15-20 MK. Phillips et al. (2005) further confirmed that the Fe XXIV line emission is the dominant contributor to emission in the TRACE 195 Å channel for flare associated high temperature features (such as hot LT emission). These bright EUV loops showed a large-scale contraction. The descending motion of X-ray LT source ceased at 02:35 UT while the EUV coronal loops continued to contract several minutes later, which we interpret as an effect of plasma cooling (from X-rays to EUV). The speeds of downward motion for EUV loops and X-ray LT source are comparable during the descending phase of X-ray LT source. Another noticeable

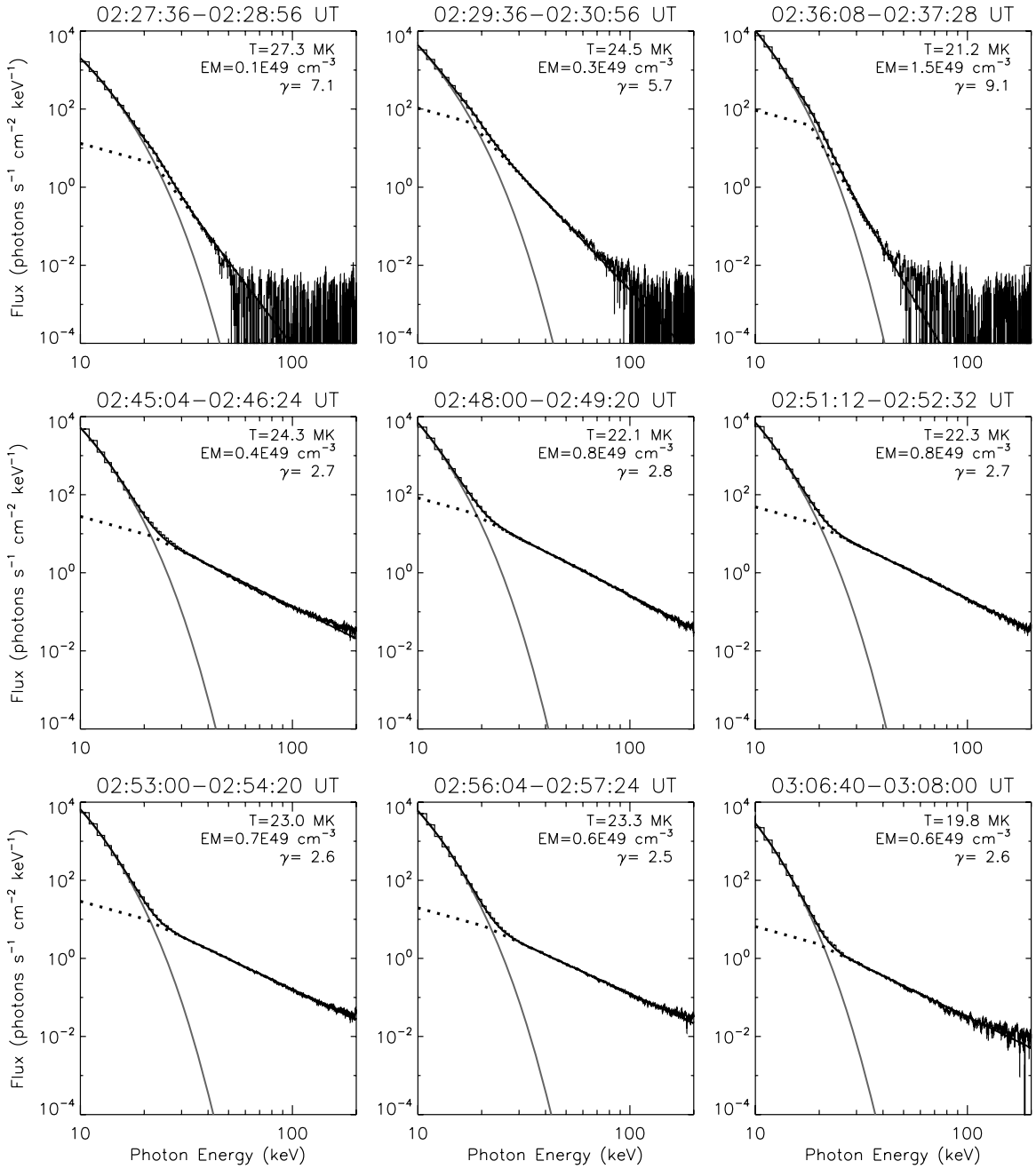

Figure 10. Spatially integrated background-subtracted *RHESSI* spectra derived during nine time intervals during the flare together with the applied spectral fits. The spectra were fitted with a thermal bremsstrahlung model (gray lines) and a functional power law with a turn-over at low energies (dotted lines). The black full lines indicate the sum of both components. The early spectra (top row) were fitted in the energy range 10–50 keV, the spectra derived during the second phase of the flare (middle and bottom rows) were fitted in the range 10–200 keV.

feature in 25–50 keV X-ray images is the appearance of two bright FP sources in this phase for a short interval (02:30:00–02:31:00).

The downward motion of LT source in the early phase of flare evolution has been established by many *RHESSI* observations (Krucker et al. 2003; Sui & Holman 2003; Sui et al. 2004; Liu et al. 2004, 2008; Ji et al. 2006; Veronig et al. 2006; Joshi et al. 2007). Some of the previously studied events also show energy-dependent structure of the LT source during the phase of altitude decrease, i.e., the higher energy sources were located higher in the corona and showed a faster speed of downward motion than lower energy sources (Sui et al. 2004; Veronig et al. 2006; Liu et al. 2008). In our event, however, the difference of LT altitude between the sources observed at low- and high-energy bands is not significant during this stage. Further, the LT altitude decrease is observed in *RHESSI* observations for ∼11 minutes, which is significantly longer than reported previously. The contraction of flaring EUV coronal loops has been reported by Li & Gan (2006), Ji et al. (2007), and Liu et al. (2009b). Li & Gan (2005) reported the shrinkage of flare loops from radio observations at 34 GHz.

Finally, we note that the duration of downward motion of the LT source is marked by high plasma temperature. *RHESSI* observations indicate that the plasma temperature reached to high values (∼27 MK) at the early stage. The temperature determined from *GOES* channels is lower (maximum temperature

$\approx$ 20 MK) and shows gradual rise with the LT shrinkage. Large difference between temperature computed from *RHESSI* and *GOES* measurements could be due to different sensitivity and response of these two instruments. This is also consistent with the fact that the observed plasma is multi-temperature. These results suggest a possible connection between LT heating and loop contraction.

3.2. The Second Phase

The flare evolution during the second phase shows impulsive HXR emission at high energies. During this interval various observational signatures in Hα, (E)UV, and HXR wavelengths can be well understood by the standard CSHKP (Carmichael 1964; Sturrock 1966; Hirayama 1974; Kopp & Pneuman 1976) model of eruptive flares. These observational features include: appearance of two parallel flare ribbons in TRACE 1600 Å and Hα images; two HXR FPs with increasing separation, one lying on each flare ribbons; growth of X-ray LT height; formation of a relatively cool loop system below the X-ray LT source at UV and Hα wavelengths connecting the flare ribbons as well as post-flare loop configuration observed in the later stages of gradual decline of X-ray intensity. *RHESSI* and *GOES* measurements suggest that there is no further increase in temperature during the second phase. The flat X-ray spectra at high energies ($\gamma < 3$) obtained during the second phase indicate strong non-thermal emission, dominated by energy released into acceleration of electrons.

The beginning of the second phase is marked by the appearance of a HXR FP source which lie on the northern UV flare ribbon. At the flare maximum, second FP source developed on the southern flare ribbon. However, the intensity of the southern FP increases continuously after the flare maximum and eventually both the FPs became of comparable brightness (Figure 6). The consistency between the timings of peaks in light curves and morphological evolution of FP sources can be understood in terms of thick-target model (Brown 1971; Hudson 1972; Syrovatskii & Shmeleva 1972) in which the X-ray production at the FPs of the loop system takes place when high-energy electrons, accelerated in the reconnection region, come along the guiding magnetic field lines and slam the denser transition region and chromospheric layers producing HXR emission via nonthermal bremsstrahlung produced by fast electrons scattered off ions. The evolution of FP sources from asymmetric to symmetric brightness can be seen as an evidence for different injection conditions of high-energy electrons along the two legs of the loop system (Siarkowski & Falewicz 2004) which could be mainly because of the highly complicated systems of loops. We find that the upward motion of 12–25 keV LT source starts at the flare maximum. This upward growth indicates progression of magnetic reconnection in the higher coronal loops rooted successively further apart from the magnetic inversion line. The beginning of the ascending motion of the X-ray LT source at the overall maximum of the HXR time profile has been reported in several flares observed by *RHESSI* (Sui & Holman 2003; Sui et al. 2004; Liu et al. 2004, 2008; Veronig et al. 2006). On the other hand, the lower loops eventually cool down (and fade away) and begin to be visible in low energies in UV and Hα lines. The structure of flaring region seen in Hα filter grams at this stage also reveals a loop system connecting two Hα flare ribbons and is very similar to the 1600 Å images. We find that intense emission is produced from the top of the Hα loops. The appearance of bright LT source in Hα emission against the solar disk was also observed in the LT event studied in Veronig et al. (2006) and Joshi et al. (2007). It is rather an unusual feature and considered as an evidence for high pressure, i.e. high density ($n \gtrsim 10^{12}$ cm^{-3}) in the observed post-flare loops (Heinzel & Karlicky 1987).

3.3. Overall Picture of the Flare Evolution

In order to interpret our observational results, we have to recall some general properties of energy accumulation before a solar flare and energy release during a flare. On the basis of data obtained by the *Hard X-ray Telescope* (*HXT*) on the satellite *Yohkoh*, Somov et al. (2002, 2003) suggested that the large-scale structure and dynamics of two-ribbon flares, as seen in HXRs, can be explained in terms of the three-dimensional reconnection at a separator in the corona. More specifically, they suggested that, before a large two ribbon flare the bases of magnetic field lines are moved by the large-scale photospheric flows of two types. First, the converging flows, i.e., the flows directed to the photospheric neutral line (PNL), create the pre-flare current layers in the corona and provided an excess of magnetic energy sufficient to produce a flare. Second, the shear flows, which are parallel to the PNL, increase the length of field lines in the corona and, therefore, produce an excess of energy too.

During a flare, both excesses of magnetic energy are released completely or partially. In this way, the model describes two kinds of apparent motions of the HXR kernels. One involves the increasing distance between the chromospheric flare ribbons (and associated HXR kernels) which results from reconnection in a coronal current layer. The other involves the approaching kernels and is associated with the relaxation of magnetic tensions generated by the photospheric shear flows before a flare. We call the latter process *shear relaxation* (for more details, see Somov 2007).

Let us clarify the general situation in terms of a specific model called "rainbow reconnection" (Somov 1986). Figure 11(a) shows the simplest presentation of a bipolar distribution of the vertical component B_z of magnetic field in the photosphere. The neutral line PNL divides the region into two zones with field polarities *N* and *S*. This region may be deformed by horizontal photospheric flows with the velocity field $\mathbf{V}$ in such a way that the PNL gradually acquires the shape of the letter *S* as shown in Figure 11(b). Beginning at a critical value of the curvature of the PNL (see Gorbachev & Somov 1988) in the magnetic field above the photosphere, calculated in the potential approximation, there appears a topologically featured field line, a separator, as illustrated in Figure 12. The separator *X* is located above the PNL like a rainbow above a river which makes a bend. The separator is the place where a reconnecting current layer can be created, and therefore the preflare energy accumulation can begin.

On the other hand, Figure 11(c) shows that a large-scale vortex-type flow generates two components of the velocity field in the photosphere: the velocity components $\mathbf{V}_\parallel$ and $\mathbf{V}_\perp$ are parallel and perpendicular to the PNL. The first component provides a shear of field lines (magnetic shear) above the PNL. The shear flow before a flare creates the longer magnetic loops which, being reconnected mainly during the first phase of a flare, provide the bright HXR kernels with a large FP separation (Figure 13). The second component $\mathbf{V}_\perp$ of the velocity field in the photosphere tends to drive reconnection in the corona. To demonstrate the basic physics in the simplest way, we consider only a central region *C* in the vicinity of the *S*-shaped neutral line PNL in Figure 11(b). Here we put the *y*-direction along the

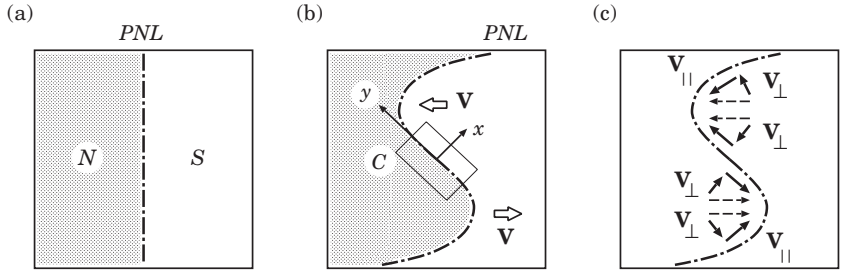

Figure 11. (a) Model distribution of a vertical component of magnetic field in the photospheric plane. (b) A large-scale vortex flow in the photosphere distorts the PNL. (c) A schematic decomposition of the velocity field **V** into the components parallel and perpendicular to the PNL.

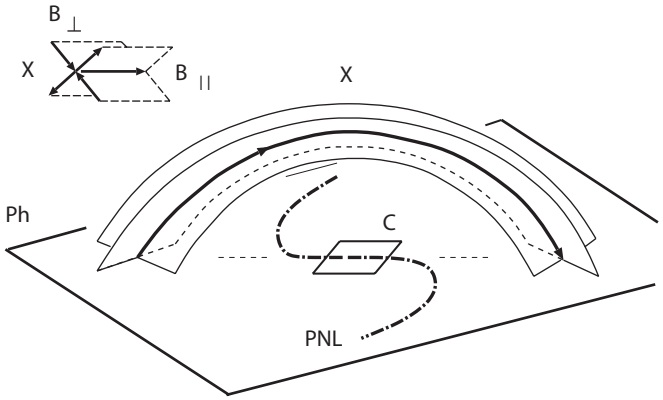

Figure 12. "Rainbow reconnection" model (Somov 1986). Separator *X* above the *S*-shaped bend of the PNL. The inset in the upper left-hand corner shows the structure of magnetic field near the top of the separator with a longitudinal component $\mathbf{B}_\parallel$.

PNL; the separator is nearly parallel to PNL as was shown in Figure 12.

Being reconnected at the separator, each magnetic field line as well as each tube of magnetic flux f is initially accelerated to high velocity ($\gtrsim$1000 km s^{-1}) inside a super-hot turbulent-current layer (SHTCL; Somov 2007, Chapter 6). Each tube of reconnected field lines, being frozen into super-hot ($T_e \gtrsim 10^8$ K) plasma, moves out of the SHTCL; in the downflow it forms a magnetic loop with properties of a collapsing magnetic trap (Somov & Kosugi 1997; Somov 2007, Chapter 7). A collapsing magnetic trap model has been first applied to one of the *RHESSI* events showing a descending LT source by Veronig et al. (2006). The longitudinal and transverse sizes of the trap decrease, causing the trapped particles to acquire an additional energy under Fermi and betatron acceleration, respectively (Somov & Bogachev 2003). The energy distribution of trapped electrons and their HXR emission can be calculated as a function of the trap length and its thickness (Bogachev & Somov 2007).

If the electrons injected into the trap from the SHTCL have a power-law energy distribution, then their spectrum remains a power-law one throughout the acceleration process for both the Fermi and betatron mechanisms. For electrons with a thermal injection spectrum, the model predicts two types of HXR coronal sources. (a) Thermal sources are formed in traps dominated by the betatron mechanism. (b) Nonthermal sources with a power-law spectrum appear when electrons are accelerated by the Fermi mechanism. With account of rare Coulomb collisions inside the trap, a double-power-low spectrum is formed from a power-law spectrum of electron injection from SHTCL (Bogachev & Somov 2009). Fermi acceleration has significant advantages in collapsing magnetic traps as compared with the betatron mechanism which mainly heats the low-energy electrons (Somov 2007, Chapter 7).

It is important to note that the emission measure of emitting fast electrons, trapped and accelerated inside the collapsing loop, initially grows slowly with decrease of the loop length $L(t)$. As calculated by Bogachev & Somov (2007), see their Figure 3(a), the emission measure reaches its maximal value only when the loop length becomes as small as of about 0.2–0.1 of its initial length $L(0)$. With further shrinkage of the loop, the emission measure decreases quickly to zero. As a consequence, the flux of HXR emission from the collapsing trap attains a maximum at approximately the same values of the remaining length of the loop (see l (t) $= L(t)/L(0) \sim 0.2$ in Figure 4(a) in Bogachev & Somov 2007). On the other hand, when the loop is just created by reconnection process at the X-point inside a thin reconnecting current layer (e.g., Ugai 2008), it is strongly stressed by magnetic tensions along magnetic field lines in the direction from the X-point to the edge of the current layer. That is why the loop shrinks and becomes less stressed. Moreover, the loop goes down less quickly with the progress of time because the magnetic stress decreases continuously. In other words, the loop becomes less non-equilibrium, more close to a state with minimal energy, i.e., the potential state (Somov 2006). In such a state, the height of the loop is naturally proportional to the distance between its feet. Therefore, it is reasonable to assume that, at the time when the collapsing loop has the maximal brightness in HXRs, the height of the LT coronal HXR sources is proportional to the distance between the conjugate FP sources in the chromosphere.

Now we shall discuss the consequences of the last assumption coming back to the rainbow reconnection model. Figure 13(a) shows different flux tubes f_1, f_2, etc. reconnected at different times t_1, t_2, etc.; here $t_2 > t_1$, etc. The first flux tube, the loop f_1 manifests two FPs P_a and P_b and a LT HXR source LT. Figure 13(a) illustrates two effects. The first one is the well-known classical effect, an increase of the distance between the flare ribbons because of reconnection in the coronal SHTCL. The displacements δx of FPs are antiparallel to the converging components $\mathbf{V}_\perp$ of the velocity field in the photosphere. This means that two flare ribbons move out from the PNL as predicted by the standard model of two-ribbon flare.

The second effect is less trivial. The displacements δy of the FPs are parallel to the PNL because of relaxation of the nonpotential component of the field created by the photospheric shear flows before a flare. So this is the magnetic shear relaxation. The displacements δy of FPs are antiparallel to the photospheric shear velocity $V_\parallel$. Since the photospheric shear mainly dominates in the vicinity of the PNL, during the first phase of a flare $\delta y \gg \delta x$.

In order to interpret our observational results related to the first phase, let us consider a magnetic loop f_1 which after the

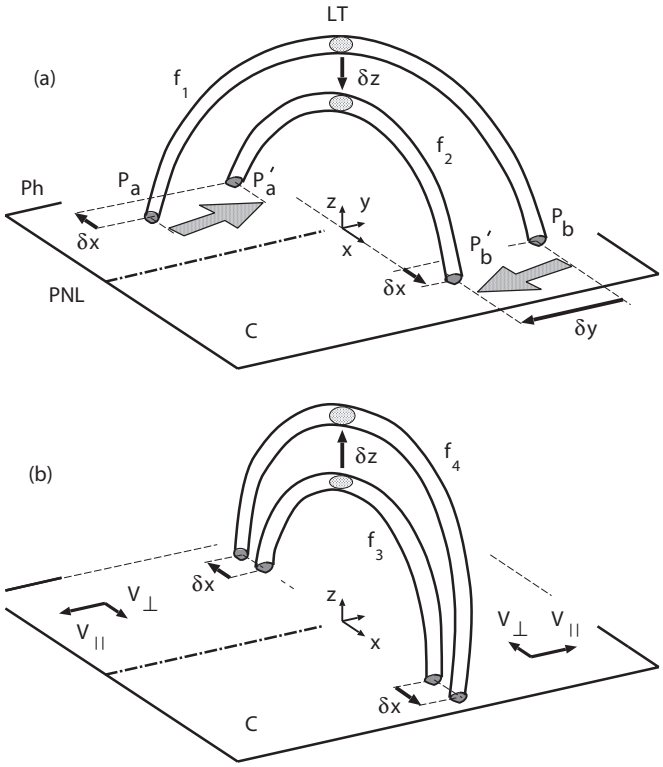

Figure 13. Schematic representation of the flare evolution in terms of the rainbow reconnection model. (a) First phase: rapidly decreasing FP separation dominates an increase of distance between flare ribbons. The LT HXR source goes down. (b) Second phase: bright HXR kernels separate in opposite directions from the PNL and from each other. The LT moves upward.

magnetic shear relaxation process evolves into loop f_2. The magnetic loop f_1 has a larger altitude of the LT HXR source (LT) because the distance between its FPs, P_a, and P_b is larger than the distance between the FPs of loop f_2, P_a', and P_b'. As a result, an apparent motion of the coronal HXR source is directed downward ($\delta z < 0$) and the two conjugate FP sources converge. The descending motion of the coronal source is typical for the first phase in the flare of 2003 October 24, as well as presumably in many other flares (see Sui & Holman 2003; Sui et al. 2004; Li & Gan 2005; Ji et al. 2006; Veronig et al. 2006; Ji et al. 2007; Joshi et al. 2007; Liu et al. 2009a). The observations of larger separation between the two conjugate X-ray FPs observed in the first phase than that in the second phase (cf. Figure 7) also seems to be consistent with our model. However, the detailed analysis FPs motion during the first phase was not possible for this event as FPs were visible for a very short time.

The second phase of a flare involves reconnection of the magnetic field lines (and flux tubes) whose FPs are located at larger distance from the PNL and, therefore, have a smaller shear or practically none as schematically illustrated by Figure 13(b). Here the apparent displacements δx of FPs are directed away from each other and from the PNL. The distance between FPs becomes larger with time, and the LT HXR source moves upward in agreement with the standard model. This seems to be fairly true for eruptive flares in the later stage when the primary energy source (i.e., reconnection site) is located high enough in the corona. It looks like that the standard model of the two-ribbon flares seems to be "asymptotically" true at later stages. However, this is not necessarily a charitable trust. Here it is noteworthy that same physical concepts concerning the photospheric motions may apply to other events such as the Bastille Day Flare of 2000 July 14, although more complicated models are required to explain the observational characteristics of such a large event (Somov et al. 2002, 2005b).

In 72 flare events analyzed by Somov et al. (2005a) on the basis of the *Yohkoh HXT* data, it was not simple to distinguish a flare with a decreasing FP separation parallel to the PNL, as discussed above, from a flare with increasing separation also parallel to the PNL, because both kinds of separation were present in the same flare. In the onset of such a flare, the FP sources move toward each other and the distance between them decreases. Then they pass through a "critical point." At this moment, the line connecting the sources is nearly perpendicular to the straight PNL; in general, we should characterize the photospheric magnetic field by a *smoothed, simplified* neutral line (*SNL*; see Gorbachev & Somov 1989) which is not a straight line. After that moment, the FP sources move away from each other with increasing separation between them (for example, the M4.4 flare on 2000 October 29 at 01:46 UT; Somov et al. 2005a, see Figure 2). Such a motion pattern seems to be similar to that one predicted by the rainbow reconnection model after the critical moment shown in Figure 13(b). Starting that moment, the shear relaxation must continue ($\delta y > 0$) if the excess of coronal magnetic tensions have not been completely released during the first phase. Otherwise the ordinary reconnection process ($\delta y = 0$) dominates during the second phase describing the ordinary energy release in terms of the classical standard model. Note that in both cases $\delta x > 0$ and, therefore, during the second phase the FP separation increases and, as a consequence, the height of the LT HXR sources increases too.

In summary, recent multi-wavelength studies of solar flares have revealed a kind of two evolutionary phases of solar flares in terms of the motion of LT source. In the initial phase (or the first phase) the LT source exhibits a downward motion for a few to several minutes and the explanation of this phase is beyond the scope of classical CHSKP scenario of eruptive flares. The analysis of 2003 October 29 M7.6 flare, presented in this paper, provides one of the clearest observations of the descending LT source with X-ray and EUV images. Recent studies have revealed another important aspect of the first phase in which the descending LT source motion in temporally associated with the converging motion of FP sources (Ji et al. 2006, 2007; Liu et al. 2009a) which is consistent with the rainbow reconnection model discussed in this paper. Ji et al. (2007) suggested another explanation of the first phase which is based on magnetic implosion conjecture (Hudson 2000) that predicts contraction of coronal field lines simultaneously with the energy release. In the framework of sheared linear force-free arcade, Ji et al. (2007) showed that the release of magnetic energy will reduce magnetic shear of the arcades and that the less sheared arcades will have smaller height and span. Liu et al. (2009a) further found that the double FPs first do move toward and then away from each other, mainly parallel and perpendicular to the PNL, respectively, and that the transition from the first to the second type of these apparent FP motions coincides with the direction reversal of the motion of the LT source. Therefore an important aspect of future investigations would be to examine the relationship between the converging motion of FP sources and the descending LT source motion for more solar flares using existing data and new observations.

We acknowledge *RHESSI* and TRACE for their open data policy. *RHESSI* and TRACE are NASA's small explorer missions. The Hα data used in this paper were obtained from Solar Tower

Telescope at Aryabhatta Research Institute of observational sciencES (ARIES), Nainital, India. This work has been supported by the "Space Weather Center Project" of KASI and KASI basic research fund. This work was partially supported by the Russian Foundation for Fundamental Research (Project No. 0802-01033-a). A.M.V. acknowledges support of the Austrian Fonds zur Förderung der wissenschaftlichen Forschung (FWF grant P20867-N16). J.L. was supported by NSF grant AST-0908344. Y.J.M has been supported by the WCU grant (No. R31-10016) funded by the Korean Ministry of Education, Science and Technology and by the Korea Research Foundation Grant funded by the Korean Government (MOEHRD, Basic Research Promotion Fund) (KRF-2008-314-C00158 and 20090071744). B.J. thanks Wei Liu for useful discussions on *RHESSI* data analysis. We sincerely acknowledge the constructive comments and suggestions of the referee of the paper.

REFERENCES

Bogachev, S. A., & Somov, B. V. 2007, Astron. Lett., 33, 54
Bogachev, S. A., & Somov, B. V. 2009, Astron. Lett., 35, 57
Brown, J. C. 1971, Sol. Phys., 18, 489
Brueckner, G. E., et al. 1995, Sol. Phys., 162, 357
Carmichael, H. 1964, in Proc. AAS-NASA Symp. 50, ed. Wilmot N. Hess (Washington, DC: NASA), 451
Gallagher, P. T., Dennis, B. R., Krucker, S., Schwartz, R. A., & Tolbert, A. K. 2002, Sol. Phys., 210, 341
Gorbachev, V. S., & Somov, B. V. 1988, Sol. Phys., 117, 77
Gorbachev, V. S., & Somov, B. V. 1989, SvA, 33, 57
Handy, B. N., et al. 1999, Sol. Phys., 187, 229
Heinzel, P., & Karlicky, M. 1987, Sol. Phys., 110, 343
Hirayama, T. 1974, Sol. Phys., 34, 323
Hudson, H., Fletcher, L., Khan, J. I., & Kosugi, T. 2004, in Astrophysics and Space Science Library, Vol. 314, Solar and Space Weather Radiophysics, ed. D. E. Gary & C. Keller (Dordrecht: Kluwer), 153
Hudson, H. S. 1972, Sol. Phys., 24, 414
Hudson, H. S. 2000, ApJ, 531, L75
Hurford, G. J., et al. 2002, Sol. Phys., 210, 61
Ji, H., Huang, G., & Wang, H. 2007, ApJ, 660, 893
Ji, H., Huang, G., Wang, H., Zhou, T., Li, Y., Zhang, Y., & Song, M. 2006, ApJ, 636, L173
Joshi, B., Manoharan, P. K., Veronig, A. M., Pant, P., & Pandey, K. 2007, Sol. Phys., 242, 143
Kopp, R. A., & Pneuman, G. W. 1976, Sol. Phys., 50, 85
Krucker, S., Hurford, G. J., & Lin, R. P. 2003, ApJ, 595, L103
Krucker, S., et al. 2008, A&AR, 16, 155
Li, Y. P., & Gan, W. Q. 2005, ApJ, 629, L137
Li, Y. P., & Gan, W. Q. 2006, ApJ, 644, L97
Li, Y. P., & Gan, W. Q. 2007, Adv. Space Res., 39, 1389
Lin, J., Soon, W., & Baliunas, S. L. 2003, New Astron. Rev., 47, 53
Lin, R. P., et al. 2002, Sol. Phys., 210, 3
Liu, W., Jiang, Y. W., Liu, S., & Petrosian, V. 2004, ApJ, 611, L53
Liu, W., Liu, S., Jiang, Y. W., & Petrosian, V. 2006, ApJ, 649, 1124
Liu, W., Petrosian, V., Dennis, B. R., & Holman, G. D. 2009a, ApJ, 693, 847
Liu, W., Petrosian, V., Dennis, B. R., & Jiang, Y. W. 2008, ApJ, 676, 704
Liu, R., Wang, H., & Alexander, D. 2009b, ApJ, 696, 121
Masuda, S., Kosugi, T., Hara, H., Tsuneta, S., & Ogawara, Y. 1994, Nature, 371, 495
Metcalf, T. R., Alexander, D., Hudson, H. S., & Longcope, D. W. 2003, ApJ, 595, 483
Pant, P. 2006, JA&A, 27, 293
Phillips, K. J. H., Chifor, C., & Landi, E. 2005, ApJ, 626, 1110
Priest, E. R., & Forbes, T. G. 2002, A&AR, 10, 313
Sakao, T. 1994, PhD thesis, Univ. Tokyo
Siarkowski, M., & Falewicz, R. 2004, A&A, 428, 219
Smith, D. M., et al. 2002, Sol. Phys., 210, 33
Somov, B. V. 1986, A&A, 163, 210
Somov, B. V. 2006, Plasma Astrophysics. Part I. Fundamentals and Practice (New York: Springer)
Somov, B. V. 2007, Plasma Astrophysics. Part II. Reconnection and Flares (New York: Springer)
Somov, B. V., & Bogachev, S. A. 2003, Astron. Lett., 29, 621
Somov, B. V., & Kosugi, T. 1997, ApJ, 485, 859
Somov, B. V., Kosugi, T., Bogachev, S. A., Sakao, T., & Masuda, S. 2005a, Adv. Space Res., 35, 1700
Somov, B. V., Kosugi, T., Hudson, H. S., Sakao, T., & Masuda, S. 2002, ApJ, 579, 863
Somov, B. V., Kosugi, T., Hudson, H. S., Sakao, T., & Masuda, S. 2003, Adv. Space Res., 32, 2439
Somov, B. V., Kosugi, T., Oreshina, I. V., & Lyubimov, G. P. 2005b, Adv. Space Res., 35, 1712
Sturrock, P. A. 1966, Nature, 211, 695
Sui, L., & Holman, G. D. 2003, ApJ, 596, L251
Sui, L., Holman, G. D., & Dennis, B. R. 2004, ApJ, 612, 546
Sui, L., Holman, G. D., White, S. M., & Zhang, J. 2005, ApJ, 633, 1175
Syrovatskii, S. I., & Shmeleva, P. O. 1972, SvA, 16, 273
Ugai, M. 2008, Phys. Plasmas, 15, 032902
Veronig, A. M., Karlický, M., Vršnak, B., Temmer, M., Magdalenić, J., Dennis, B. R., Otruba, W., & Pötzi, W. 2006, A&A, 446, 675
Warren, H. P., & Reeves, K. K. 2001, ApJ, 554, L103